Topological Defects in Carbon Nanocrystals

Vladimir A. Osipov

Bogoliubov Laboratory of Theoretical Physics, Joint Institute for Nuclear Research, 141980 Dubna, Moscow region, Russia. osipov@thsun1.jinr.ru

1 Introduction

Topology and geometry have many applications in the modern condensed matter physics (see, e.g., the books [1, 2]) . The purpose of this brief review is to present some bright examples of using topology and geometry in a study of a new interesting class of carbon materials – carbon nanoparticles. The discovery of these cage-like molecules has attracted considerable attention of both experimentalists and theorists due to unique physical properties that are directly related to their exotic geometry. Moreover, there is reason to believe that an infinite variety of both carbon-based and some other materials with particular nanoscale shapes and forms can be produced, therefore increasing the significance of geometrical methods [3] in theoretical studies.

An additional interest to carbon nanoparticles originates from the fact that the exotic geometry is accompanied by topological defects. Notice that topologically nontrivial objects play the important role in various physically interesting systems. It will suffice to mention the 't Hooft-Polyakov monopole in the non-Abelian Higgs model, instantons in quantum chromodynamics, solitons in the Skyrme model, Nielsen-Olesen magnetic vortices in the Abelian Higgs model, etc. (see, e.g., [4]). Notice that similar objects are known in condensed matter physics as well. For instance, vortices in liquids and liquid crystals, solitons in low-dimensional systems (e.g., in magnetics, linear polymers, and organic molecules) as well as the famous Abrikosov magnetic vortices in superconductors are the matter of common knowledge. Mathematically, all these objects appear in the framework of nonlinear models as partial solutions of strongly nonlinear equations. An important point is that all the solutions are topologically stable and belong to nontrivial homotopic sectors.

It should be noted that elastic media also leave room for topological defects known as dislocations and disclinations. Disclinations in liquid crystals are one of the best-studied cases. In particular, the known exact 'hedgehog' solution has been obtained within the continuum model of nematics. It is interesting that a hedgehog-like solution was also found for a point 4π disclination within the framework of the gauge model [5]. An important advantage of the gauge model follows from the fact that it is similar to the known field theory models, first of all to the non-Abelian and Abelian Higgs models, where

topological objects are studied well. Taking into account this similarity, two exact static solutions for linear disclinations have been found [6, 7, 8].

It is now well understood that the modern problems of condensed matter physics call for using of new theoretical methods. As we show here, a theoretical description of variously shaped carbon nanocrystals requires involving of differential geometry, topology, and gauge theory. These methods are not typical for condensed matter theory though widely used in the field theory and gravity.

2 Geometry and Topology of Carbon Nanoparticles

The high flexibility of carbon allows producing variously shaped carbon nanostructures: fullerenes, nanotubes, nanohorns, cones, toroids, graphitic onions, etc. In some sense, the carbon nanoparticles mediate between the molecular and bulk phases and can be considered as a third form of carbon along with diamond and graphite. Historically, the fullerenes C_{60} (nicknamed also as Buckminsterfullerene or 'bucky ball') were first discovered in 1985 [9]. They are tiny molecular cages of carbon having 60 atoms and making up the mathematical shape called a truncated icosahedron (12 pentagons and 20 hexagons). Although the amount of C_{60} actually being produced in the experiment was very small, right away these curious molecules attracted attention of theorists. In 1990, the adaptation of arc technique for carbon rods gives a possibility to make C_{60} in gram quantities [10]. Since then, in the process of graphite vaporization there were produced variously shaped fullerene molecules. The more spherical of them are the C_{60} molecule and its generalizations like C_{240} and C_{540} molecules. Others are either slightly (like the C_{70} (see Fig. 1)) or remarkably deformed.

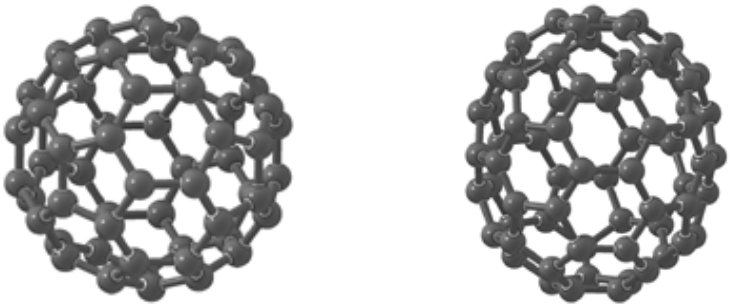

Fig. 1. The fullerene C_{60} (on the left) and C_{70} molecules

Soon after the fullerenes, other interesting carbon structures were discovered. First of all, carbon nanotubes of different diameters and helicity [11]

were produced. It turns out that single-walled carbon nanotubes can be twisted, flattened, and bent around to form sharp corners. These distortions do not cause them to break (see Fig. 2). The mechanical, magnetic, and especially electronic properties of carbon nanotubes are found to be very specific (see, e.g., [12]). For example, the nanotube can be either metallic or semiconducting depending on its diameter and helicity (see discussion below).

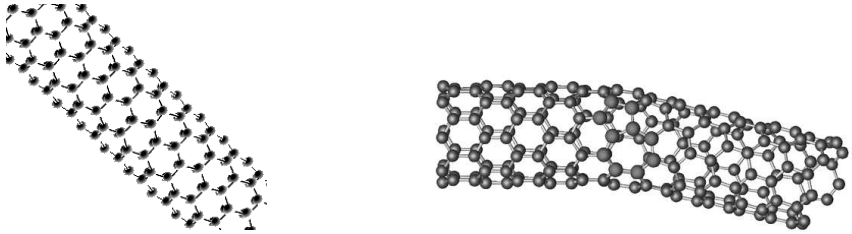

Fig. 2. Carbon nanotubes

Carbon 'onions' have also been found and they can be considered as carbon cages one inside the other [13]. The tubes and onions are likely to be composed of hexagonal and pentagonal carbon rings just like the fullerenes. However, the structures having heptagonal rings are also possible. There has been much progress in recent years in producing toroids [14], cones [15, 16] (see Figs. 3,4), nanohorns [17], boxes [18], and helically coiled graphite [19].

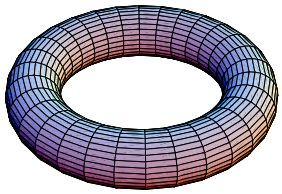

Fig. 3. Torus

One can expect that even more exotic configurations can be produced in experiment (see, e.g., Fig. 5). Indeed, theoretically the closed (without dangling bonds) fullerenes and nanotubes exhibiting high topologies (from genus 5 to genus 21) were suggested in [20]. This follows from the known Euler's theorem that relates the number of vertices, edges and faces of an object. For the hexagonal carbon lattice it can be written in the form [20]

$$...2n_4 + n_5 - n_7 - 2n_8... = \sum (6 - x)n_x = \chi = 12(1 - g), \qquad (1)$$

where n_x is the number of polygons having x sides, χ is the Euler characteristic which is a geometrical invariant related to the topology of the structure,

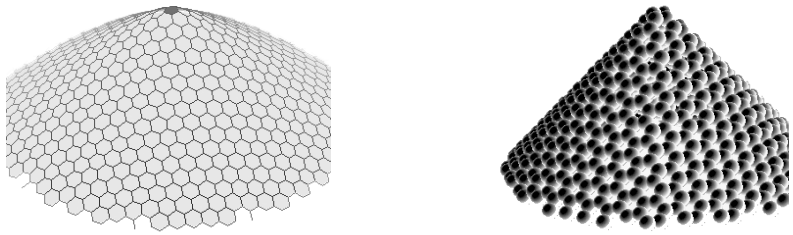

Fig. 4. Nanocones containing one (left) and two (right) pentagons at the apex

and g is the genus or a number of handles of an arrangement. So, for a sphere $g = 0$, a torus has $g = 1$ while for two 'sticked' torii in Fig. 5 one has $g = 2$. According to (1) there is no contribution to the Gaussian curvature for $x = 6$. This means that two-dimensional carbon lattice consisting only of hexagons is flat. On the contrary, to obtain a nontrivial shape one has to introduce some additional polygons. For example, in order to make a fullerene with genus zero we need additionally twelve pentagons. In general, the Euler's theorem allows to determine all the possible graphitic structures. As was mentioned in [20], in accordance with (1) the complex structures with no pentagons (no positive Gaussian curvature) can be constructed if the genus is increased. In particular, an existence of the new stable family of fullerene-like structures (holey-balls and holey-tubes) which have high genus and no pentagonal rings was predicted in [20].

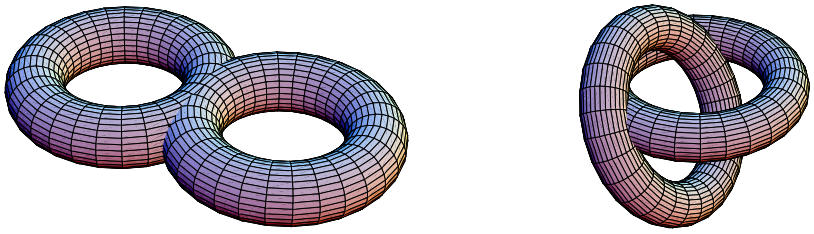

Fig. 5. Exotic configurations

By their nature, pentagons (as well as other polygons with $x \neq 6$) in a graphite sheet are topological defects. In particular, fivefold coordinated particles are orientational 60° disclination defects in the otherwise sixfold coordinated triangular lattice. This can be understood by realizing that a pentagon can be inserted in the hexagonal lattice by a cut-and-glue procedure typical for disclination defects. Namely, one has to cut out a 60° sector from a graphene (a single layer of graphite) sheet and then glue together the two cut sides of the sheet. Moreover, if the departure from the flat surface is allowed, a cone whose apex angle is directly related to the disclination angle will be generated. Pentagonal defects in cones can therefore be considered as apical

disclinations, and the opening angle is directly connected to the Frank index of the disclination. A cone's apex may consist of a combination of ring defects. Because of the symmetry of the graphite sheet, only five types of cones can be created from a continuous sheet of graphite. The total disclinations of all these cones are multiplies of 60°, corresponding to the presence of a given number (n) of pentagons at the apices. It is important to mention that carbon nanocones with the cone angles of 19°, 39°, 60°, 85°, and 113° have been observed in a carbon sample [16]. Notice that these angles might correspond to 300°, 240°, 180°, 120°, and 60° disclinations in graphite, respectively. Disks (n=0) and one-open-end nanotubes (n=6) have also been observed in the same sample [16]. This case was theoretically studied in [21, 22, 23]. At the same time, cones with apex angles of 30°, 50°, and 70° have also been found [24, 20]. These angles are forbidden within the above scenario. In [24, 25] the appearance of such cones was explained in terms of an open cone model. Another possibility gives a creation of partial disclinations. As is known, a finite graphite sheet with disclinations will be buckled to screen its energy [26]. In this case, one of the allowed geometries is the hyperboloid.

It should be noted that the presence of topological defects in the elastic medium changes the topology of space, a simple connected region becomes multiply connected whenever there are defects. As a result, the physical characteristics of quantum particles moving in defect medium can be modified in comparison with the defect free case. Indeed, the Aharonov-Bohm-like (AB-like) effect in dislocated crystals (called 'phase-dismatching') was predicted in [30]. It was found that the Schrödinger equation for a tight-binding electron is reduced to the AB-like equation in the presence of a screw dislocation (see also [31, 32]). In experiment, the effects of Berry's geometrical phase were established in analyzing the high-energy electron diffraction from a screw dislocation [33].

Among other effects it is necessary to note the prediction of the AB-like electron scattering due to disclinations [6, 34], an electron localization near topological defects [35, 36] as well as a formation of the polaron-type states near dislocations [37]. Notice that a possibility of the solid state realization of the AB effect was earlier suggested in metals [27, 28] and in dielectrics [29]. It has been shown that the AB effect results in oscillations of physical characteristics (transport properties, magnetic susceptibility) with a certain fundamental period $\Phi_0 = hc/ne$ where $n = 1$ for pure metals and $n = 2$ for disordered metals and dielectrics.

One would expect some new physical phenomena arising from nontrivial topology of carbon nanoparticles. It is interesting to note in this connection that an important role of topology has recently been discovered in experiments with niobium and selenium. In particular, a Möbius strip (see Fig. 6) of single microcrystals $NbSe_3$ has been produced by twisting a ribbon of material through 180° and joining its two ends, resulting in a distinct one-sided topology [38]. In a sense, these crystals can be considered as global disclina-

tions. It was established that the electronic properties of the Möbius crystals are modified in comparison with the ring configuration. Namely, the temperature of charge-density-wave phase transition was observed to be 4K lower than this in the ring. There is reason to believe that this effect is pure topological in its origin. Evidently, topologically nontrivial crystal forms offer a new route to study topological effects in solid state physics.

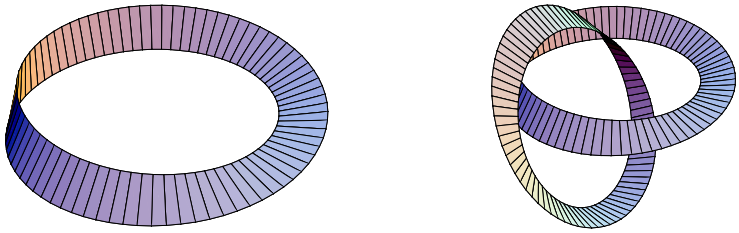

Fig. 6. Möbius stripe (left) and a more exotic configuration

3 Electronic Properties

Among the most unique features of carbon nanoparticles are their electronic properties. Electronic states in nanotubes, fullerenes, nanocones, nanohorns as well as in other carbon configurations are the subject of an increasing number of experimental and theoretical studies. They already find a use for the development of modern nanoscale electronic devices: flat panel displays, nano-switches, molecular memory devices, transistors, electron field emitters, etc. It has been predicted and later observed in experiment that bending or stretching a nanotube change its band structure changing therefore the electrical properties: stretched nanotubes become either more or less conductive. Moreover, a nanotube's chiral angle (the angle between the axis of its hexagonal pattern and the axis of the tube) determines whether the tube is metallic or semiconducting (see, e.g., [12]). This finding could allow to build nanotube-based transducers sensitive to tiny forces.

Interesting changes in the electronic properties arise from topological defects. The peculiar electronic states due to topological defects have been observed in different kinds of carbon nanoparticles by scanning tunneling microscopy (STM). For example, STM images with five-fold symmetry (due to pentagons in the hexagonal graphitic network) have been obtained in the C_{60} fullerene molecule [39]. The peculiar electronic properties at the ends of carbon nanotubes (which include several pentagons) have been probed experimentally in [40, 41]. Recently, the electronic structure of a single disclination has been revealed on an atomic scale by STM [42] where the enhanced charge

density at the disclination, which was located at the apex of the conical protuberance of the graphitic particle, has been experimentally clarified.

The problem of peculiar electronic states near the pentagons in curved graphite nanoparticles was the subject of intensive theoretical studies in fullerenes [43, 44], nanotubes [45], nanohorns [46], and cones [21, 47]. In particular, an analysis within the effective-mass theory has shown that a specific $\sqrt{3} \times \sqrt{3}$ superstructure induced by pentagon defects can appear in nanocones [48]. This prediction has been experimentally verified in [42]. A recent study [23] within both tight-binding and *ab initio* calculations shows a presence of sharp resonant states in the region close to the Fermi energy. The strength and the position of these states with respect to the Fermi level was found to depend sensitively on the number and the relative positions of the pentagons constituting the conical tip. In particular, a prominent peak which appears just above the Fermi level was found for the nanocone with three symmetrical pentagons (which corresponds to a 60° opening angle or, equivalently, to 180° disclination). A similar result has been recently obtained in the framework of the gauge-theory approach [47]. Notice also that localized cap states in nanotubes have been recently studied in [49].

It is interesting to note that the problem of specific electronic states at the Fermi level due to disclinations is similar to that of the fermion zero modes for planar systems in a magnetic field. Generally, zero modes for fermions in topologically nontrivial manifolds have been of current interest both in the field theory and condensed matter physics. As was revealed, they play a major role in getting some insight into understanding anomalies [50] and charge fractionalization that results in unconventional charge-spin relations (e.g. the paramagnetism of charged fermions) [51] with some important implications for physics of superfluid helium (see, e.g., review [52]). $3D$ space-time Dirac equation for massless fermions in the presence of the magnetic field was found to yield $N-1$ zero modes in the N-vortex background field [53]. As it was shown in [44], the problem of the local electronic structure of fullerene is closely related to Jackiw's analysis [53]. An importance of the fermion zero modes was also discussed in the context of the high-temperature chiral superconductors [54, 55, 56].

3.1 Theory: Basic Assumptions

Investigation of the electronic structure requires formulating a theoretical model describing electrons on arbitrary curved surfaces with disclinations taken into account. An important ingradient of this model can be provided by the self-consistent effective-mass theory describing the electron dynamics in the vicinity of an impurity in graphite intercalation compounds [57]. The most important fact found in [57] is that the electronic spectrum of a single graphite plane linearized around the corners of the hexagonal Brillouin zone coincides with that of the Dirac equation in (2+1) dimensions. This finding stimulated formulation of some field-theory models for Dirac fermions on

hexatic surfaces to describe electronic structure of variously shaped carbon materials: fullerenes [44], nanotubes [45, 49], and cones [21, 22].

The effective-mass theory for a two-dimensional graphite lattice is equivalent to the $\boldsymbol{k}\cdot\boldsymbol{p}$ expansion of the graphite energy bands about the $\boldsymbol{K}$ point in the Brillouin zone when the intercalant potential is equal to zero. In fact, there are two kinds of sublattice points in a unit cell (two degenerate Bloch eigenstates at $\boldsymbol{K}$) and the electron wave function can therefore be approximated by

$$\Psi(\boldsymbol{k},\boldsymbol{r}) = f_1(\boldsymbol{\kappa})e^{i\boldsymbol{\kappa}\boldsymbol{r}}\Psi_1^S(\boldsymbol{K},\boldsymbol{r}) + f_2(\boldsymbol{\kappa})e^{i\boldsymbol{\kappa}\boldsymbol{r}}\Psi_2^S(\boldsymbol{K},\boldsymbol{r})$$

where $\boldsymbol{k} = \boldsymbol{K} + \boldsymbol{\kappa}$. Keeping the terms of the order of $\boldsymbol{\kappa}$ in the Schrödinger equation results in a secular equation for the amplitudes $f_{1,2}(\boldsymbol{\kappa})$, which after diagonalization finally yields the two-dimensional Dirac equation (see, for details, Ref. [57])

$$i\gamma^\mu\partial_\mu\psi(\boldsymbol{r}) = E\psi(\boldsymbol{r}). \tag{2}$$

Here γ^μ are the Dirac matrices that in 2D reduce to the conventional Pauli matrices, the energy E is measured relative to the Fermi energy, and the two-component wave function ψ represents two graphite sublattices. As mentioned in [57], the $\boldsymbol{k}\cdot\boldsymbol{p}$ approximation essentially amounts to replacing the graphite bands by conical dispersions at the Fermi energy.

For our purpose, we need a generalization of (2) incorporating both a disclination field and a nontrivial background geometry. A possible description of disclinations on arbitrary two-dimensional elastic surfaces is offered by the gauge approach [58]. In accordance with the basic assumption of this approach, disclinations can be incorporated in the elasticity theory Lagrangian by introducing a compensating $U(1)$ gauge fields W_μ. It is important that the gauge model admits exact vortex-like solutions for wedge disclinations [58] thus representing a disclination as a vortex of elastic medium. The physical meaning of the gauge field is that the elastic flux due to rotational defect (that is directly connected with the Frank vector (see the next section)) is completely determined by the circulation of the W_μ field around the disclination line. In the gauge theory context, the disclination field can be straightforwardly incorporated in (2) by the standard substitution $\partial_\mu = \partial_\mu - iW_\mu$.

Within the linear approximation to gauge theory of disclinations (which amounts to the conventional elasticity theory with linear defects), the basic field equation that describes the $U(1)$ gauge field in a curved background is given by

$$D_\mu F^{\mu k} = 0, \quad F^{\mu k} = \partial^\mu W^k - \partial^k W^\mu, \tag{3}$$

where covariant derivative $D_\mu := \partial_\mu + \Gamma_\mu$ involves the Levi-Civita (torsion-free, metric compatible) connection

$$\Gamma^k_{\mu\lambda} := (\Gamma_\mu)^k_\lambda = \frac{1}{2}g^{kl}\left(\frac{\partial g_{l\lambda}}{\partial x^\mu} + \frac{\partial g_{\mu l}}{\partial x^\lambda} - \frac{\partial g_{\mu\lambda}}{\partial x^l}\right), \tag{4}$$

with $g_{\mu k}$ being the metric tensor on a Riemannian surface Σ with local coordinates $x^\mu = (x^1, x^2)$. For a single disclination on an arbitrary elastic surface, a singular solution to (3) is found to be [58]

$$W^k = -\nu \varepsilon^{k\lambda} D_\lambda G(x, y), \tag{5}$$

where

$$D_\mu D^\mu G(x^1, x^2) = 2\pi \delta^2(x^1, x^2)/\sqrt{g}, \tag{6}$$

with $\varepsilon_{\mu k} = \sqrt{g}\epsilon_{\mu k}$ being the fully antisymmetric tensor on Σ, $\epsilon_{12} = -\epsilon_{21} = 1$. It should be mentioned that eqs. (3-6) self-consistently describe a defect located on an arbitrary surface [58].

To describe fermions in a curved background, we need a set of orthonormal frames $\{e_\alpha\}$ which yield the same metric, $g_{\mu\nu}$, related to each other by the local $SO(2)$ rotation,

$$e_\alpha \to e'_\alpha = \Lambda^\beta_\alpha e_\beta, \quad \Lambda^\beta_\alpha \in SO(2).$$

It then follows that $g_{\mu\nu} = e^\alpha_\mu e^\beta_\nu \delta_{\alpha\beta}$ where e^μ_α is the zweibein, with the orthonormal frame indices being $\alpha, \beta = \{1, 2\}$, and coordinate indices $\mu, \nu = \{1, 2\}$. As usual, to ensure that physical observables are independent of a particular choice of the zweinbein fields, a local $so(2)$ valued gauge field ω_μ must be introduced. The gauge field of the local Lorentz group is known as the spin connection. For the theory to be self-consistent, the zweibein fields must be chosen to be covariantly constant [59]:

$$\mathcal{D}_\mu e^\alpha_\nu := \partial_\mu e^\alpha_\nu - \Gamma^\lambda_{\mu\nu} e^\alpha_\lambda + (\omega_\mu)^\alpha_\beta e^\beta_\nu = 0,$$

which determines the spin connection coefficients explicitly

$$(\omega_\mu)^{\alpha\beta} = e^\alpha_\nu D_\mu e^{\beta\nu}. \tag{7}$$

Finally, the Dirac equation (2) on a surface Σ in the presence of the $U(1)$ external gauge field W_μ is written as

$$i\gamma^\alpha e_\alpha^{\ \mu}(\nabla_\mu - iW_\mu)\psi = E\psi, \tag{8}$$

where $\nabla_\mu = \partial_\mu + \Omega_\mu$ with

$$\Omega_\mu = \frac{1}{8}\omega_\mu^{\ \alpha\ \beta}[\gamma_\alpha, \gamma_\beta] \tag{9}$$

being the spin connection term in the spinor representation.

Notice that the general analytical solution to (8) is known only for chosen geometries. One of them is the cone [21, 22]. For the sphere and the hyperboloid, which are of interest here, there were used some approximations. In particular, asymptotic solutions at small r (which allow us to study electronic states near the disclination line) were considered in [47]. For this reason, the numerical calculations for all three geometries were performed in [60]. The results of both analytical and numerical studies will be presented in the next section.

4 Spherical Molecules

4.1 The Model

To describe a sphere, we employ the polar projective coordinates $x^1 = r, x^2 = \varphi$; $0 \leq r < \infty, 0 \leq \varphi < 2\pi$ with R being the radius of the sphere. In these coordinates, the metric tensor becomes

$$g_{rr} = 4R^4/(R^2 + r^2)^2,\ g_{\varphi\varphi} = 4R^4 r^2/(R^2 + r^2)^2,\ g_{r\varphi} = g_{\varphi r} = 0, \qquad (10)$$

so that

$$\sqrt{g} := \sqrt{\det ||g_{\mu\nu}||} = 4R^4 r/(R^2 + r^2)^2.$$

Nonvanishing connection coefficients (4) take the form

$$\Gamma^r_{rr} = -\frac{2r}{R^2 + r^2}, \quad \Gamma^r_{\varphi\varphi} = -r\frac{R^2 - r^2}{R^2 + r^2}, \quad \Gamma^\varphi_{r\varphi} = \frac{1}{r}\frac{R^2 - r^2}{R^2 + r^2},$$

and the general representation for the zweibeins is found to be

$$e^1{}_r = e^2{}_\varphi = 2R^2 \cos\varphi/(R^2 + r^2),\ e^1{}_\varphi = -e^2{}_r = -2R^2 \sin\varphi/(R^2 + r^2),$$

which in view of (7) gives

$$\omega^{12}_r = \omega^{21}_r = 0, \quad \omega^{12}_\varphi = -\omega^{21}_\varphi = 2r^2/(R^2 + r^2) =: 2\omega. \qquad (11)$$

The following solution to (5) and (6) can be easily found

$$G = \log r; \quad W_r = 0, \quad W_\varphi = \nu, \quad r \neq 0.$$

Locally, it describes a topological vortex on the Euclidean plane, which confirms the observation that disclinations can be viewed as vortices in elastic media. Notice that the elastic flux is actually characterized by the Frank vector $\boldsymbol{\omega}$, $|\boldsymbol{\omega}| = 2\pi\nu$ with ν being the Frank index. The elastic flow through a surface on the sphere is given by the circular integral

$$\frac{1}{2\pi}\oint \boldsymbol{W}\, d\boldsymbol{r} = \nu.$$

Generally, there are no restrictions on the value of the winding number ν apart from $\nu > -1$ for topological reasons. This means that the elastic flux is 'classical' in its origin; i.e., there is no quantization (in contrast to the magnetic vortex). However, if we take into account the symmetry group of the underlying crystal lattice, the possible values of ν become 'quantized' in accordance with the group structure (e.g., $\nu = 1/6, 1/3, 1/2, ...$ for the hexagonal lattice). It is interesting to note that in some physically interesting applications vortices with the fractional winding number have already been considered (see, e.g., the discussion in [54]). Notice also that a detailed theory of magnetic vortices on a sphere has been presented in [61].

In $2D$, the Dirac matrices can be chosen as the Pauli matrices: $\gamma^1 = -\sigma^2, \gamma^2 = \sigma^1$ and (9) reduces to

$$\Omega_\varphi = i\omega\sigma^3. \tag{12}$$

As a result, the Dirac operator $\hat{\mathcal{D}} := i\gamma^\alpha e_\alpha^\mu(\nabla_\mu + iW_\mu)$ on the two-sphere becomes

$$\hat{\mathcal{D}} = \hat{\mathcal{D}}^\dagger = \frac{r^2+R^2}{2R^2}\begin{bmatrix} 0 & e^{-i\varphi}(-\partial_r + \frac{i\partial_\varphi+\nu}{r} + \frac{\omega}{r}) \\ e^{i\varphi}(\partial_r + \frac{i\partial_\varphi+\nu}{r} - \frac{\omega}{r}) & 0 \end{bmatrix}. \tag{13}$$

For massless fermions σ^3 serves as a conjugation matrix, and the energy eigenmodes are symmetric with respect to $E = 0$ ($\sigma^3\psi_E = \psi_{-E}$). The generator of the local Lorentz transformations $\Lambda_\alpha^\beta \in SO(2)$ takes the form $-i\partial_\varphi$, whereas the generator of the Dirac spinor transformations $\rho(\Lambda)$ is

$$\Sigma_{12} = \frac{i}{4}[\gamma_1, \gamma_2] = \frac{1}{2}\sigma^3.$$

The total angular momentum of the $2D$ Dirac system is therefore given by

$$L_z = -i\partial_\varphi + \frac{1}{2}\sigma^3,$$

which commutes with the operator (13). Consequently, the eigenfunctions are classified with respect to the eigenvalues of $J_z = j + 1/2,\ j = 0, \pm1, \pm2, ...$, and are to be taken in the form

$$\psi = \begin{pmatrix} u(r)e^{i\varphi j} \\ v(r)e^{i\varphi(j+1)} \end{pmatrix}. \tag{14}$$

As is follows from (13) the spin connection term can be taken into account by redefining the wave function as

$$\psi = \tilde{\psi}\sqrt{R^2+r^2}, \tag{15}$$

which reduces eigenvalue problem (8) to

$$\begin{aligned} \partial_r\tilde{u} - \frac{(j-\nu)}{r}\tilde{u} &= \tilde{E}\tilde{v}, \\ -\partial_r\tilde{v} - \frac{(j+1-\nu)}{r}\tilde{v} &= \tilde{E}\tilde{u}, \end{aligned} \tag{16}$$

where $\tilde{E} = 2R^2E/(R^2+r^2)$.

4.2 Extended Electron States

Let us consider an approximate solution to (16). The point is that, because we are mainly interested in electronic states near the disclination line, we can

restrict our consideration to the case of small r. In this case, a solution to (16) (with (15) taken into account) is found to be

$$\begin{pmatrix} u \\ v \end{pmatrix} = A \begin{pmatrix} J_\eta(2Er) \\ \pm J_{\bar{\eta}}(2Er) \end{pmatrix} \tag{17}$$

where $\eta = \pm(j-\nu)$, $\bar{\eta} = \pm(j-\nu+1)$, and A is a normalization factor. Therefore, there are two independent solutions with $\eta(\bar{\eta}) > 0$ and $\eta(\bar{\eta}) < 0$. Notice that respective signs $\pm$ in (17) correspond to states with $E > 0$ and $E < 0$. As already noted, σ^3 serves as the conjugation matrix for massless fermions, and the energy eigenmodes are symmetric with respect to $E = 0$. One can therefore consider either case, for instance, $E > 0$.

The important restrictions come from the normalization condition

$$\int (|u|^2 + |v|^2)\sqrt{g}dx^1 dx^2 = 1. \tag{18}$$

From (17), it follows that $A^2 \sim E$. On the other hand, the integrand in (18) must be nonsingular at small Er. This imposes a restriction on possible values of j. Namely, for $\eta, \bar{\eta} > 0$ one obtains $j - \nu > -1/2$, and for $\eta, \bar{\eta} < 0$ one has $j - \nu < -1/2$. As is seen, possible values of j do not overlap at any ν.

In the vicinity of a pentagon, the electron wave function reads

$$\begin{pmatrix} u \\ v \end{pmatrix} \sim \begin{pmatrix} E^{1/2+\eta} r^\eta, \\ E^{1/2+\bar{\eta}} r^{\bar{\eta}} \end{pmatrix}. \tag{19}$$

In particular, in the leading order, one obtains $\Psi \sim \sqrt{E}$, $\Psi \sim E^{1/3} r^{-1/6}$, and $\Psi \sim E^{1/6} r^{-1/3}$ for $\nu = 0,\ 1/6,\ 1/3$, respectively. Because the local density of states diverges as $r \to 0$, it is more appropriate to consider the total density of states on a patch $0 < r \leq \delta$ for small δ, rather than the local quantities. For this, the electron density should be integrated over a small disk $|r| < \delta$ (recall that r, φ are stereographically projected coordinates on the sphere). The result is

$$D(E,\delta) \propto \begin{cases} (E\delta)\delta, & \nu = 0; \\ (E\delta)^{2/3}\delta, & \nu = 1/6, 5/6; \\ (E\delta)^{1/3}\delta, & \nu = 1/3, 2/3; \\ \delta, & \nu = 1/2; \end{cases} \tag{20}$$

For the defect free case ($\nu = 0$) we obtain the well-known behavior of the total DOS in the δ disk given by $D(E,\delta) \sim E\delta^2$ (in accordance with the previous analysis [57]). For $\nu = 1/6, 1/3, 2/3, 5/6$, the low-energy total DOS has a cusp which drops to zero at the Fermi energy. Most intriguing is the case where $\nu = 1/2$ and a region of a nonzero DOS across the Fermi

level is formed. This implies local metallization of graphite in the presence of 180° disclination. In the fullerene molecule, however, there are twelve 60° disclinations, and therefore, the case $\nu = 1/6$ is actually realized.

4.3 Numerical Results

The numerical calculations for the case of sphere were presented in a recent paper [60]. As a starting point, the analytical asymptotic solutions found in the previous section are considered. The initial value of the parameter r is defined as $r = 10^{-4}$. It is worth noting that the choice of the boundary conditions does not influence the behavior of the calculated wave functions and only the starting point depends on it. A dimensionless substitution $x = Er$ is used. The normalized numerical solutions to (16) are given in Fig. 7. The parameters are chosen to be $E = 0.01$ and $R = 1$. Notice that here we present

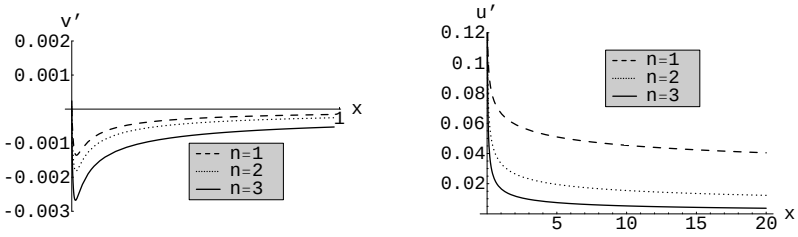

Fig. 7. The solutions $v'(x), u'(x)$ for different n.

the solutions for dotted values $v'(= \tilde{v})$ and $u'(= \tilde{u})$. The local DOS is shown schematically in Figs. 8,9 for different n. Notice that the Fig. 9 describes also the dependence of the local DOS on a position of the maximum value of integrand in (18)(which actually characterizes the numerically calculated localization point of an electron).

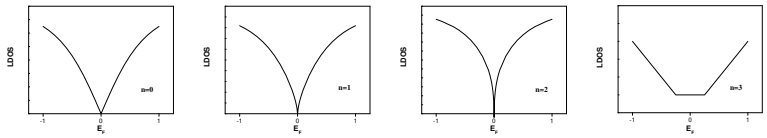

Fig. 8. Schematic densities of states near the Fermi energy in the case of sphere.

Here and below $\delta = 0.1$. Notice that in fact the choice of the value of δ does not influence the characteristic behavior of LDOS. As is seen, the DOS has a cusp which drops to zero at the Fermi energy. The case $n = 3$ becomes

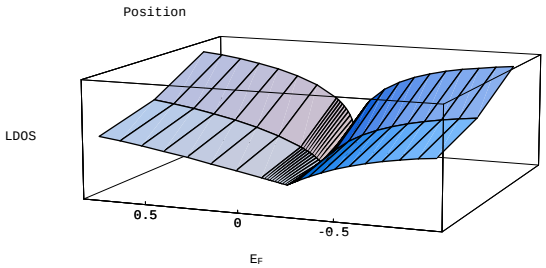

Fig. 9. 3d schematic plotting of the DOS near the Fermi energy for $n = 0, 1, 2$ (going from the front side to the back side).

distinguished. Let us emphasize once more that in the fullerene molecule there are twelve 60° disclinations, so that the case $n = 1$ is actually realized.

4.4 Zero-energy Modes

An interesting issue to be addressed is the existence of zero-energy modes. For the two-sphere, this problem can be solved exactly (see [53, 44]). Namely, for $E = 0$, (16) reduces to

$$\begin{aligned} \partial_r \tilde{u}_0 - \frac{(j-\nu)}{r}\tilde{u}_0 = 0, \\ -\partial_r \tilde{v}_0 - \frac{(j+1-\nu)}{r}\tilde{v}_0 = 0. \end{aligned} \tag{21}$$

One can construct self-conjugate solutions $\binom{\tilde{u}_0}{0}$ and $\binom{0}{\tilde{v}_0}$ where

$$\tilde{u}_0 = Ar^{j-\nu}, \qquad \tilde{v}_0 = Ar^{-(j-\nu+1)}. \tag{22}$$

The normalization condition

$$\int |\psi_0|^2 \sqrt{g} dr d\varphi = 1 \tag{23}$$

yields

$$2\pi A^2 \int_0^\infty \frac{4R^4 r^{2l}}{R^2 + r^2} r dr = 1 \tag{24}$$

where $l = j - \nu$ for u_0 and $l = -(j - \nu + 1)$ for v_0. Finally, $A^2 = \sin \pi\bar{\eta}/4\pi^2 R^{2(1+\bar{\eta})}$ for u_0 and $A^2 = -\sin \pi\eta/4\pi^2 R^{2(1-\eta)}$ for v_0, respectively. Notice that the restriction $-1 < j - \nu < 0$ serves to avoid divergence in (23). In the defect free case ($\nu = 0$), this yields no zero modes on a sphere. Notice that this agrees with a general observation that the Dirac operator can have no zero modes on a manifold with an everywhere positive Ricci scalar curvature $\mathcal{R}$. Indeed, one easily obtains $\hat{\mathcal{D}}^2 = \Delta + \mathcal{R}/4$, where the Laplace-Beltrami

operator Δ has nonnegative eigenvalues. For the two-sphere $\mathcal{R} = 1/R^2$, and therefore, $\hat{\mathcal{D}}^2 > 0$.

For $\nu = 1/6$, which is of our interest here, the only possible value of j is $j = 0$, so that $u_0 \sim r^{-1/6}$ and $v_0 \sim r^{-5/6}$ near the disclination line. Thus, our analysis shows that two normalizable zero modes can exist on a sphere in the presence of a disclination vortex. Let us note that this conclusion agrees with [43] (where different continuum model was formulated) and differs from [53, 44] where either u_0 or v_0 were found to be normalizable. The reason is that in [53, 44] the external gauge field was assumed to be well behaved at the origin whereas here singular solutions are also admitted.

The total density of states on a patch $0 < r \leq \delta$ becomes

$$D(\delta) \propto \begin{cases} \delta^{1/3}, \nu = 1/6, 5/6; \\ \delta^{2/3}, \nu = 1/3, 2/3; \\ \delta, \quad \nu = 1/2; \end{cases} \tag{25}$$

As is seen, this behavior differs from (20) thus allowing to recognize the zero-eigenvalue states in experiment.

5 Nanocones

5.1 The Model

In the polar coordinates $(r, \varphi) \in R^2$ a cone can be regarded as an embedding

$$(r, \varphi) \to (ar\cos\varphi,\ ar\sin\varphi,\ cr), \quad 0 < r < 1, 0 \leq \varphi < 2\pi,$$

with a and c being the cone parameters. From this, the components of the induced metric can be easily read off:

$$g_{rr} = a^2 + c^2, \qquad g_{\varphi\varphi} = a^2 r^2, \qquad g_{r\varphi} = g_{\varphi r} = 0. \tag{26}$$

The opening angle of a cone, θ, is determined by $\sin(\theta/2) = a/\sqrt{a^2 + c^2}$. Because the cone itself appears when one or more sectors are removed from graphene, all possible angles are divisible by $\pi/3$. Therefore, the Frank index of the apical disclination can be specified by $\nu = 1 - \sin(\theta/2)$. At $\nu = 0$ one gets a flat graphene sheet ($\theta = \pi$). For convenience, we introduce a parameter $\xi = 1 + c^2/a^2$, so that $\sin(\theta/2) = 1/\sqrt{\xi}$ and $1/\sqrt{\xi} = 1 - \nu$.

Nonvanishing connection coefficients (4) are now given by

$$\Gamma^r_{\varphi\varphi} = -r/\xi, \quad \Gamma^\varphi_{r\varphi} = \Gamma^\varphi_{\varphi r} = 1/r.$$

The general representation for the zweibeins is found to be

$$e^1{}_r = a\sqrt{\xi}\cos\varphi, \quad e^1{}_\varphi = -ar\sin\varphi, \quad e^2{}_r = a\sqrt{\xi}\sin\varphi, \quad e^2{}_\varphi = ar\cos\varphi,$$

which in view of (7) gives

$$\omega_r^{12} = \omega_r^{21} = 0, \quad \omega_\varphi^{12} = -\omega_\varphi^{21} = 1 - 1/\sqrt{\xi} =: 2\omega. \tag{27}$$

The external gauge potential is then found to be $W_r = 0$, $W_\varphi = \nu$, and the Dirac operator on the cone takes the form

$$\hat{\mathcal{D}} = \begin{bmatrix} 0 & e^{-i\varphi}\left(-\frac{\partial_r}{\sqrt{a^2+c^2}} + \frac{1}{ar}(i\partial_\varphi + \nu + \omega)\right) \\ e^{i\varphi}\left(\frac{\partial_r}{\sqrt{a^2+c^2}} + \frac{1}{ar}(i\partial_\varphi + \nu - \omega)\right) & 0 \end{bmatrix}.$$

Making the substitution

$$\psi = \tilde{\psi} r^\alpha, \; \alpha = \sqrt{\xi}\omega,$$

one reduces the eigenvalue problem (8) to

$$\begin{aligned} \partial_r \tilde{u} - \frac{\sqrt{\xi}}{r}(j - \nu)\tilde{u} &= \tilde{E}\tilde{v}, \\ -\partial_r \tilde{v} - \frac{\sqrt{\xi}}{r}(j + 1 - \nu)\tilde{v} &= \tilde{E}\tilde{u}, \end{aligned} \tag{28}$$

where $\tilde{E} = \sqrt{\xi} a\, E$.

5.2 Electron States

Unlike the previous case of the two-spere, the cone is essentially a flat manifold (the scalar curvature $\mathcal{R} = 0$ everywhere on the cone, except for the origin), and as a result, (28) allows an exact solution. Namely, the general solution to (28) is found to be [22]

$$\begin{pmatrix} \tilde{u} \\ \tilde{v} \end{pmatrix} = A r^{-\alpha} \begin{pmatrix} J_\eta(\tilde{E}r) \\ \pm J_{\bar{\eta}}(\tilde{E}r) \end{pmatrix}, \tag{29}$$

where $\eta = \pm(\sqrt{\xi}(j - \nu + 1/2) - 1/2)$, and $\bar{\eta} = \pm(\sqrt{\xi}(j - \nu + 1/2) + 1/2)$. As earlier, we consider the case where $E > 0$. Normalization condition (18) takes the form

$$2\pi\sqrt{\xi} a^2 A^2 \int_0^1 (J_\eta^2(\tilde{E}r) + J_{\bar{\eta}}^2(\tilde{E}r)) r dr = 1. \tag{30}$$

The normalization factor can be extracted from the asymptotic formula for Bessel functions at large arguments. Indeed, in our case, $\bar{\eta} - \eta = 1$ so that $J_\eta^2 + J_{\bar{\eta}}^2 \to 2/\pi\tilde{E}r$ for $\tilde{E}r \gg 1$. Substituting this in (30) yields $A^2 = E/4a$. Clearly, (30) must be nonsingular at small r. This imposes a restriction on possible values of j. Namely, for $\eta, \bar{\eta} > 0$ one gets $j > -1$ (i.e., $j = 0, 1, 2...$) while for $\eta, \bar{\eta} < 0$ one has $j < -2\nu$ ($j = -1, -2, ...$ at $\nu < 1/2$).

We are interested in the electron states near the apex of a cone. As it follows directly from (29), for small r the wave functions behave as

$$\begin{pmatrix} u \\ v \end{pmatrix} \sim \begin{pmatrix} E^{1/2+\eta} r^{\eta}, \\ E^{1/2+\bar{\eta}} r^{\bar{\eta}} \end{pmatrix}, \tag{31}$$

In the leading order, one obtains

$$\tilde{\Psi} \sim E^{(1-2\nu)/2(1-\nu)} r^{-\nu/(1-\nu)}.$$

In particular, we obtain $\tilde{\Psi} \sim \sqrt{E}$, $\tilde{\Psi} \sim E^{2/5} r^{-1/5}$, and $\tilde{\Psi} \sim E^{1/4} r^{-1/2}$ for $\nu = 0,\ 1/6,\ 1/3$, respectively.

Finally, the total density of states on the patch $0 < r \leq \delta$ is found to be

$$D(E,\delta) \propto \begin{cases} E^{(1+2\nu)/(1-\nu)} \delta^{(\nu+2)/(1-\nu)}, & \eta, \bar{\eta} > 0; \\ E^{(1-2\nu)/(1-\nu)} \delta^{(2-3\nu)/(1-\nu)}, & \eta, \bar{\eta} < 0. \end{cases} \tag{32}$$

It should be stressed that, according to (32), a specific behavior of $D(E,\delta)$ occurs only for $\nu = 1/2$ where $D \sim E^0 \delta$. This agrees with a finding in [23], where the prominent peak just above the Fermi level was found for the nanocone with three symmetric pentagons (180° disclination). In the leading order, it follows from (32) that

$$D(E,\delta) \propto \begin{cases} E\delta^2, & \nu = 0; \\ E^{4/5}\delta^{9/5}, & \nu = 1/6; \\ E^{1/2}\delta^{3/2}, & \nu = 1/3; \\ \delta, & \nu = 1/2; \end{cases} \tag{33}$$

As is seen, the extended states with a nonzero density of states at E_F appear only at $\nu = 1/2$.

To examine the electron states at the Fermi energy, one has to return to (28) and set $E = 0$. The solution reads

$$u_0 = A r^{-\frac{1}{2}+\widetilde{j}} \sqrt{\xi}, \qquad v_0 = B r^{-\frac{1}{2}-\widetilde{j}} \sqrt{\xi}, \tag{34}$$

where $\widetilde{j} = j - \nu + 1/2$. A simple analysis shows that for $j = 0$ both u_0 and v_0 are normalizable on the cone of a finite size. Both solutions are singular. For $\nu = 1/6$ one gets $|u_0|^2 \sim r^{-1/5}/a^2$ and $|v_0|^2 \sim r^{-9/5}/a^2$. For any other j, either u_0 or v_0 is found to be normalizable and the solutions become nonsingular. As before, for singular states one can consider the total DOS. It is easy to find that $D \sim \delta^{1/5}$ for u_0 and $D \sim \delta^{9/5}$ for v_0. This result differs from [48] where, although in a different framework, the states on a finite cone with a single-pentagon defect have been found at the Fermi energy (these states decay away from the apex as $|\psi|^2 \sim r^{-2/5}$). At the same time, our study confirms the principal conclusion in [48, 62] that the states contributing to the

nonzero DOS at the Fermi energy exhibit a power-law behavior for a single-pentagon defect. Notice also that in monolayer graphite of infinite length ($a \to \infty$) there are no zero-energy electronic states on a single disclination. It should be emphasized that this conclusion agrees with the results of numerical calculations [62] where the local density of states at the Fermi level was found to be zero for five-membered rings (pentagons). Notice also that for $\nu = 1/2$, $D \sim \delta$ for both u_0 and v_0.

5.3 Numerical Results

It is interesting to present the results of numerical calculations [60]. The normalized numerical solutions to (28) for different n are shown in Fig. 10. The parameters are chosen to be: $E = 0.01$, $a = 1$, and $c = 1$. The 'total' DOS near the Fermi energy for the case of the cone is illustrated schematically in Figs. 11.

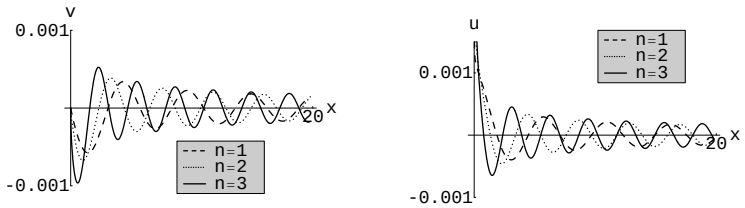

Fig. 10. The solutions $v(x), u(x)$ for different n.

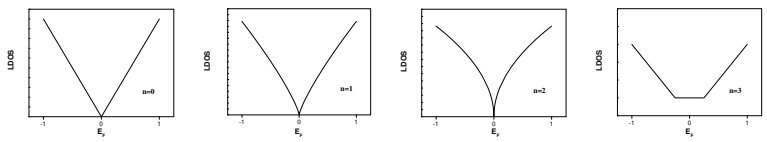

Fig. 11. Schematic densities of states near the Fermi energy in the case of cone.

One can see that the 'total' DOS has a cusp which drops to zero at the Fermi energy. It should be stressed that a specific behavior takes place only for $n = 3$ where a nonzero DOS near the Fermi energy is found.

6 Hyperboloid Geometry

6.1 The Model

The upper half of a hyperboloid can be regarded as the embedding

$$(\chi,\varphi)\to(a\sinh\chi\cos\varphi, a\sinh\chi\sin\varphi, c\cosh\chi),\quad 0\le\chi<\infty, 0\le\varphi<2\pi,$$

From these, the components of the induced metric can be obtained as

$$g_{\chi\chi}=a^2\cosh^2\chi+c^2\sinh^2\chi,\quad g_{\varphi\varphi}=a^2\sinh^2\chi,\quad g_{\varphi\chi}=g_{\chi\varphi}=0, \tag{35}$$

which, for the nonvanishing connection coefficients, yields

$$\Gamma^{\chi}_{\chi\chi}=\frac{(a^2+c^2)\sinh 2\chi}{2g_{\chi\chi}},\quad \Gamma^{\chi}_{\varphi\varphi}=-\frac{a^2\sinh 2\chi}{2g_{\chi\chi}},\quad \Gamma^{\varphi}_{\varphi\chi}=\Gamma^{\varphi}_{\chi\varphi}=\coth\chi. \tag{36}$$

In a rotating $SO(2)$ frame, the zweibeins become

$$e^1{}_{\chi}=\sqrt{g_{\chi\chi}}\cos\varphi,\ e^2{}_{\chi}=\sqrt{g_{\chi\chi}}\sin\varphi,\ e^1{}_{\varphi}=-a\sinh\chi\sin\varphi,\ e^2{}_{\varphi}=a\sinh\chi\cos\varphi, \tag{37}$$

which in view of (7) gives the spin connection coefficients

$$\omega^{12}_{\chi}=\omega^{21}_{\chi}=0,\quad \omega^{12}_{\varphi}=-\omega^{21}_{\varphi}=\frac{1}{2}\left[1-\frac{a\cosh\chi}{\sqrt{g_{\chi\chi}}}\right]=:\omega, \tag{38}$$

and therefore,

$$\Omega_{\varphi}=i\omega\sigma^3. \tag{39}$$

The external gauge potential in this case is found to be $W_\chi=0$, $W_\varphi=\nu$, and the Dirac operator on the hyperboloid takes the form

$$\hat{\mathcal{D}}=\begin{bmatrix} 0 & e^{-i\varphi}\left(-\frac{\partial_\chi}{\sqrt{g_{\chi\chi}}}+\frac{1}{a\sinh\chi}(i\partial_\varphi+\nu+\omega)\right)\\ e^{i\varphi}\left(\frac{\partial_\chi}{\sqrt{g_{\chi\chi}}}+\frac{1}{a\sinh\chi}(i\partial_\varphi+\nu-\omega)\right) & 0\end{bmatrix}.$$

It can be verified that $\hat{\mathcal{D}}=\hat{\mathcal{D}}^\dagger$.

The substitution

$$\tilde{\psi}=\psi\sqrt{\sinh\chi}$$

reduces the eigenvalue problem (8) to

$$\begin{aligned}\partial_\chi\tilde{u}-\sqrt{\coth^2\chi+b^2}\,\tilde{j}\tilde{u}&=\tilde{E}\tilde{v},\\ -\partial_\chi\tilde{v}-\sqrt{\coth^2\chi+b^2}\,\tilde{j}\tilde{v}&=\tilde{E}\tilde{u},\end{aligned} \tag{40}$$

where $\tilde{E}=\sqrt{g_{\chi\chi}}\,E$, $b=c/a$, and $\tilde{j}=j-\nu+1/2$.

6.2 Electron States

To study electronic states on the hyperboloid one has to analyze (40). As for the sphere, let us consider the behavior of the electron states near the apex which is the case of small χ. One obtains

$$\begin{aligned} \partial_\chi \tilde{u} - \frac{\tilde{j}}{\chi}\tilde{u} &= Ea\tilde{v}, \\ -\partial_\chi \tilde{v} - \frac{\tilde{j}}{\chi}\tilde{v} &= Ea\tilde{u}, \end{aligned} \tag{41}$$

with the obvious solution

$$\tilde{u} = A\sqrt{Ea\chi}J_{|j-\nu|}(Ea\chi), \quad \tilde{v} = A\sqrt{Ea\chi}J_{|j-\nu+1|}(Ea\chi),$$

As is seen, this is exactly the case of a sphere, which should not be surprising, because these two manifolds are locally diffeomorphic. Evidently, the 'total' (on the disk $|r| < \delta$) DOS is the same as on the sphere. However, for hyperboloid the problem is more intricate due to the requirement to fulfill the normalization condition (see the numerical calculations below).

An interesting situation arises for the zero-energy solution. Let us consider the zero-energy modes setting $E = 0$ in (41). The general solution is found to be

$$\begin{aligned} \tilde{u}(\chi) &= A\left[(k\cosh\chi + \Delta)^{2k}\,\frac{\Delta - \cosh\chi}{\Delta + \cosh\chi}\right]^{\frac{\tilde{j}}{2}}, \\ \tilde{v}(\chi) &= A\left[(k\cosh\chi + \Delta)^{2k}\,\frac{\Delta - \cosh\chi}{\Delta + \cosh\chi}\right]^{-\frac{\tilde{j}}{2}} \end{aligned} \tag{42}$$

where $k = \sqrt{1+b^2}$, $\Delta = \sqrt{1 + k^2\sinh^2\chi}$. An important restriction comes from the normalization condition which on a finite hyperboloid yields $\tilde{j} > -1/2$ for $u(\chi)$ and $\tilde{j} < 1/2$ for $v(\chi)$. One can see that for $-1/2 < \tilde{j} < 1/2$ both $u(\chi)$ and $v(\chi)$ are normalizable simultaneously. For the zero-energy mode, the total DOS on a finite hyperboloid is found to be the same as on the sphere (see (25)).

Although the local electronic structures are similar on the hyperboloid and the sphere, there is a principal global distinction. In proving this, let us consider an unbounded hyperboloid (full locus). In this case, one has to take into account additional restrictions at the upper limit of the integral in (18). One obtains $-1/2 < \tilde{j} < -1/2k$ for $u(\chi)$ and $1/2k < \tilde{j} < 1/2$ for $v(\chi)$. Thus, either $u(\chi)$ or $v(\chi)$ becomes normalizable on the hyperboloid of infinite volume. One can see that as $(c/a) \to 0$ a normalizable solution does not exist. In fact, under this condition the hyperboloid is changing over to a plane. Consequently, our results are in accordance with the planar case. The

total density of states on an infinite hyperboloid for a variety of defects is as follows:

$$D(\delta) \propto \begin{cases} \delta^{1/3},\ \nu = 1/6, 5/6;\ c/a > \sqrt{5}/2 \\ \delta^{2/3},\ \nu = 1/3, 2/3;\ c/a > 2\sqrt{2}. \end{cases} \tag{43}$$

Notice that normalizable zero-energy states do not exist for the defect with $\nu = 1/2$ nor for the defect-free case $\nu = 0$. The most important conclusion from our consideration is that there is a possibility for the true zero-mode fermion state on the hyperboloid. As we have shown, the normalized zero-mode states on both the sphere and the cone exist only for a finite system size and disappear in the infinite-size limit. For an infinite hyperboloid, a normalized zero-energy electron state can exist in the presence of a disclination flux.

6.3 Numerical Results

The more clear difference comes from the numerical study. The results of the numerical calculations are shown in Fig. 12 where the parameters are chosen to be $E = 0.01$, $a = 1$, and $c = 1$. Notice that the starting point in this case was chosen to be $y = 0.01$. As can be seen, for the hyperboloid the

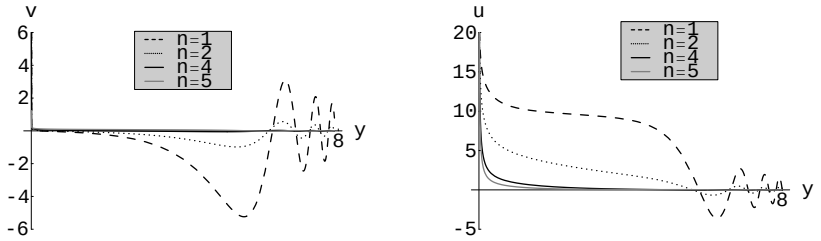

Fig. 12. Solutions $v(y), u(y)$ for different n.

electron eigenfunctions behave similar to the sphere near the disclination line and remarkably differ at large distances. In addition, there is a problem with the normalization of the solution for hyperboloid. Actually, the integrand is found to be constantly growing with increasing parameter y. Due to this problem (coming from the hyperboloid geometry itself) it is impossible to perform numerical calculations of the DOS.

To compare the behavior of the solutions $u(u')$ for every kind of the geometries the combined pictures are shown in Fig. 13 for $n = 1, 2$. It can be seen that the solutions for the sphere and the hyperboloid have a similar behaviour near the disclination line at small $x(y)$, as it was already discussed. Let us note that the solution for $u(u')$ is found to be of the decisive impor-

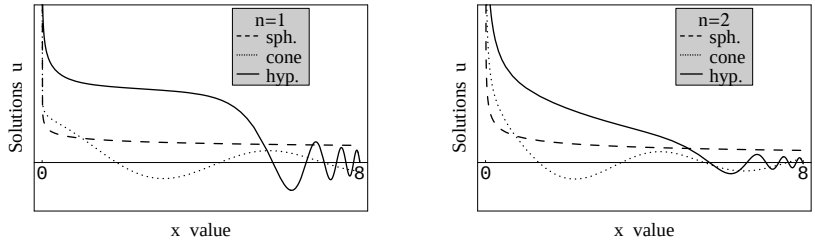

Fig. 13. The schematic pictures for $u(x)$ for three geometries in the case of $n = 1, 2$.

tance in the final results for all three geometries, which is consistent with the previous analytical results. The choice of the parameters (R, c, a) does not influence the main characteristics of the calculated wave functions.

In summary, the numerical calculations confirm the finding that the pentagonal defects in graphite nanoparticles markedly modify the low-energy electronic structure. This is evident from both the exact form of wave functions and the local density of electron states. As is seen from Fig. 9, in the case of sphere the local DOS increases with a distance from the disclination line for defects with $n = 1, 2$. The low-energy total DOS has a characteristic cusp at the Fermi energy for any number of pentagons except $n = 3$ where the enhanced charge density at the Fermi energy is found.

7 Conclusion

There are many interesting applications of geometrical and topological methods to actual problems of modern condensed matter physics. As shown above, the physics of carbon nanoparticles is one of the striking examples. The geometry and topology is found to influence the main physical characteristics of graphite nanoparticles, first of all, their electronic properties. The topological defects (disclinations) appear as generic defects in closed carbon structures. For 180° disclination (three pentagons), the electronic density of states is found to be remarkably increased. Physically this means local metallization, thus suggesting some important applications of nanocone-based structures in microelectronic devices. First of all, such a remarkable increase of the DOS must provoke the corresponding enhancement of the field emission current, thereby decreasing the threshold voltage for emitted electrons. It should be noted that this conclusion agrees well with the results in [23], where the prominent peak appearing just above the Fermi level was established in a nanocone with three pentagons at the apex. It was proposed that such peculiar nanocones are good candidates for nanoprobes in scanning probe microscopy and excellent candidates for field-emission devices. As was also mentioned in [23], the nanocones with free pentagons at the tip have the

highest probability of nucleation and are frequently observed [16]. It is expected that localized states at the Fermi level may give rise to materials with novel electronic and magnetic properties.

It should be emphasized that a big variety of closed graphitic structures is generally expected to be produced. Therefore, the theoretical study of various topologically nontrivial objects as well as of topological defects in graphite and other materials is of great importance. There is reason to believe that an application of geometrical and topological methods to condensed matter physics will result in considerable progress in the near future.

I would like to thank Profs. A.M. Kosevich, M.I. Monastyrskii, and B. Zhilinskii for fruitful discussions during the workshop. The main results presented in this short review have been obtained in co-authorship with Drs. E.A. Kochetov, M. Pudlak, and R. Pincak whom I am very grateful. This work has been supported by the Science and Technology Department of Moscow region and the Russian Foundation for Basic Research under grant No. 01-02-97021.

References

1. M.I. Monastyrskii: *Topology of Gauge Fields and Condensed Matter*, (Plenum, New York 1993)
2. J.F. Sadoc (ed): *Geometry in Condensed Matter Physics*, (World Scientific, 1990)
3. B.A. Dubrovin, S.P. Novikov, A.T. Fomenko: *Modern Geometry - Methods and Applications: The Geometry of Surfaces, Transformation Groups and Fields*, (Springer-Verlag, New York 1993).
4. R. Rajaraman: *Solitons and Instantons*, (North-Holland, Amsterdam 1982)
5. V.A. Osipov: Phys.Lett. A **146**, 67 (1990)
6. V.A. Osipov: Phys. Lett. A **164**, 327 (1992)
7. V.A. Osipov: J. Phys. A: Math. Gen. **26**, 1375 (1993)
8. V.A. Osipov: Phys. Lett. A **193**, 97 (1994)
9. H.W. Kroto, J.R. Heath, S.C. O'Brien et al: Nature **318**, 162 (1985)
10. W. Kratschmer, L.D. Lamb, K. Fostiropoulos et al: Nature **347**, 354 (1990)
11. S. Iijima: Nature **354**, 56 (1991)
12. T.W. Ebbesen: Physics Today, (June) 26 (1996)
13. D. Ugarte: Nature **359**, 707 (1992)
14. J. Liu, H.J. Dai, J.H. Hafner et al: Nature **385**, 780 (1997)
15. M. Ge, K. Sattler: Chem. Phys. Lett. **220**, 192 (1994)
16. A. Krishnan, E. Djuardin, M.M.J. Treacy et al: Nature **388**, 451 (1997)
17. S. Iijima, M. Yudasaka, R. Yamada et al: Chem. Phys. Lett. **309**, 165 (1999)
18. Y. Saito, T. matsumoto: Nature **392**, 237 (1998)
19. S. Amenlinckx, X.B. Zhang, D. Berbaerts: Science **265**, 635 (1994)
20. H. Terrones, M. Terrones: Carbon **36**, 725 (1998)
21. P.E. Lammert, V.H. Crespi: Phys. Rev. Lett. **85**, 5190 (2000)
22. V.A. Osipov, E.A. Kochetov: JETP Lett. **73**, 631 (2001)
23. J.-C. Charlier, G.-M. Rignanese: Phys. Rev. Lett. **86**, 5970 (2001)

24. N.A. Kiselev, J. Sloan, D.N. Zakharov et al: Carbon, **36**, 1149 (1998).
25. H. Terrones, T. Hayashi, M. Munoz-Navia et al: Chem. Phys. Lett. **343**, 241 (2001).
26. D.R. Nelson, L. Peliti: J.Phys. (Paris) **48** 1085 (1987)
27. I.O. Kulik: JETP Lett. **11** 275 (1970)
28. B.L. Altshuler, A.G. Aronov, B.Z. Spivak: JETP Lett. **33** 94 (1981)
29. E.N. Bogachek, I.V. Krive, I.O. Kulik, et al: JETP **97** 603 (1990)
30. K. Kawamura: Z.Physik B. **29** 101 (1978); ibid. **30** 1 (1978)
31. R. Bausch, R. Schmitz, L.A. Turski: Phys. Rev. B **59**, 13491 (1999)
32. C. Furtado, V.B. Bezerra, F. Moraes: Europhys. Lett. **52**, 1 (2000)
33. D.M. Bird, A.R. Preston: Phys.Rev.Lett. **61** 2863 (1988)
34. S. Azevedo, F. Moraes: Phys. Lett. A **246**, 374 (1998)
35. V.A. Osipov: J. Phys. A: Math. Gen. **24**, 3237 (1991)
36. C. Furtado, F. Moraes: Phys. Lett. A **188**, 394 (1994)
37. V.A. Osipov: Phys. Rev. B **51**, 8614 (1995)
38. S. Tanda, T. Tsuneta, Y. Okajima et al: Nature (London) **417**, 397 (2002)
39. J.G. Hou, J. Yang, H. Wang et al: Phys. Rev. Lett. **83**, 3001 (1999)
40. D.L. Carroll, P. Redlich, P.M. Ajayan et al: Phys. Rev. Lett. **78**, 2811 (1997)
41. P. Kim, T.W. Odom, J.-L. Huang et al: Phys. Rev. Lett. **82**, 1225 (1999)
42. B. An, S. Fukuyama, K. Yokogawa et al: Appl. Phys. Lett. **78**, 3696 (2001)
43. J. González, F. Guinea, M.A.H. Vozmediano: Phys. Rev. Lett. **69** 172 (1992); Nucl.Phys. B **406** 771 (1993)
44. V.A. Osipov, E.A. Kochetov: JETP Lett. **72**, 199 (2000)
45. C.L. Kane, E.J. Mele: Phys. Rev. Lett. **78**, 1932 (1997)
46. S. Berber, Y.-K. Kwon, D. Tománek: Phys. Rev. B **62**, R2291 (2000)
47. V.A. Osipov, E.A. Kochetov, M. Pudlak: JETP **96**, 140 (2003)
48. K. Kobayashi: Phys. Rev. B **61**, 8496 (2000)
49. T. Yaguchi, T. Ando: J.Phys.Soc.Jpn. **71** 2224 (2002)
50. R. Jackiw, C. Rebbi: Phys. Rev. D **16**, 1052 (1977)
51. R. Jackiw, J.R. Schrieffer: Nucl. Phys. B **190**, 253 (1981)
52. M.M. Salomaa, G.E. Volovik: Rev. Mod. Phys. **59** 533 (1987)
53. R. Jackiw: Phys. Rev. D **29**, 2375 (1984)
54. G.E. Volovik: JETP Lett. **63** 763 (1996)
55. G.E. Volovik: JETP Lett. **70** 609 (1999)
56. G.E. Volovik: JETP Lett. **70** 792 (1999)
57. D.P. DiVincenzo, E.J. Mele: Phys. Rev. B **29**, 1685 (1984)
58. E.A. Kochetov, V.A. Osipov: J.Phys. A: Math.Gen. **32**, 1961 (1999)
59. M.B. Green, J.H. Schwartz, E. Witten: *Superstring theory*, v.2 (Cambridge 1988).
60. R. Pincak, V.A. Osipov: Phys. Lett. A (2003) in press
61. B.A. Ovrut, S. Tomas: Phys.Rev. D **43** 1314 (1991)
62. R. Tamura, M. Tsukada: Phys. Rev. B **49** 7697 (1994)